Published in final edited form as:
Chem Phys Lett. 2011 May 27; 508(4-6): 314–319. doi:10.1016/j.cplett.2011.04.043.

Modulation of cross polarization in motionally averaged solids by Variable Angle Spinning NMR

Catalina A. Espinosa[a], **Pierre Thureau**[b], **Rebecca A. Shapiro**[a], **Ilya M. Litvak**[a], and **Rachel W. Martin**[a,c,*]

[a]Department of Chemistry, University of California, Irvine 92697-2025

[b]Laboratoire Chimie Provence, UMR 6264, Université Aix-Marseille I, II et III-CNRS, Marseille 13397, France

[c]Department of Molecular Biology and Biochemistry, University of California, Irvine 92697-2025

Abstract

In systems where the dipolar couplings are partially averaged by molecular motion, cross-polarization is modulated by sample spinning. The cross-polariation efficiency in Variable Angle Spinning (VAS) and Switched Angle Spinning (SAS) experiments on mobile samples is therefore strongly dependent on the spinning angle. We describe simulations and experimental measurements of these effects over a range of spinning angles from 0° to 90°.

Keywords

solid-state NMR; cross polarization; variable angle spinning; switched angle spinning; adamantane

1. Introduction

Cross-polarization (CP), in which magnetization is transferred from abundant, high gyromagnetic-ratio nuclei to rare, low gyromagnetic-ratio nuclei via the dipolar couplings [1], is a nearly ubiquitious building block in solid-state NMR experiments. In the static case, CP occurs when the RF fields for two nuclei, *I* and *S*, e.g. ^{1}H and ^{13}C, are matched in the rotating frame according to the Hartmann-Hahn condition. In practice, CP is most useful under magic angle spinning (MAS) [2], where it is well known that the cross-polarization intensity is modulated by the spinning frequency, giving rise to a sideband pattern where $|\omega_{1S} \pm \omega_{1I}| = n\,\omega r$, where ω_{1S} and ω_{1I} are the RF fields applied to the *S* and *I* spins, and ω_r is the spinning frequency. At the magic angle, the $n = \pm 1$ and $n = \pm 2$ conditions dominate the matching profile and the center band is suppressed [3, 4].

Spinning off the magic angle reintroduces anisotropic interactions, providing an alternative to pulse sequence-based recoupling schemes. Variable angle spinning (VAS) [5, 6] and switched angle spinning (SAS) experiments yield correlations between isotropic spectra and

*rwmartin@uci.edu.

anisotropic spectral information such as chemical shift anisotropy [7, 8, 9] or heteronuclear dipolar couplings [10]. VAS requires that the entire pulse sequence be repeated at each angle, and in many SAS experiments the preparation period and mixing time take place off the magic angle, with only the signal collection done under MAS. Most previous SAS studies have focused on strongly coupled systems, i.e. rigid solids where the modulation is negligible, particularly for slow to moderate spinning rates. In this case, an acceptable signal may be obtained at any spinning angle without altering the CP match condition. One exception is the dynamic angle spinning experiment using CP between a spin 1/2 nucleus and the central transition of a quadrupole at 0° followed by detection at the magic angle [11], since in this case the time dependence of the first-order quadrupolar interaction interferes with the polarization transfer when the spinning axis deviates from zero degrees. For systems with attenuated dipolar couplings, the CP match condition likewise strongly depends on the spinning axis as demonstrated by Sardashti and Maciel for SAS between 0° and 90° [12].

This type of measurement has the potential to be useful at the interface between solid-state and solution NMR, where the dipolar couplings are partially averaged, particularly in the context of new methods for assignment of proteins in oriented samples where it is beneficial to obtain spectra at both 0° and 90° [13]. VAS and SAS methods have been applied to strongly ordered liquid crystals, in which the director alignment changes with the spinning axis, modulating the anisotropic interactions [14, 15, 16, 17]. Scaled dipolar couplings and CSAs can also be measured using stretched polymer gels to provide weak alignment; in this case the variable angle experiment does not require sample spinning [18]. VAS experiments on bicelles have been performed with direct detection of ^{2}H [19], or ^{31}P [20, 21], and SAS experiments used to simplify the spectra of organic molecules in a liquid crystal [22, 23] and peptides in bicelles [24] have used direct detection of ^{19}F or ^{1}H, respectively, without polarization transfer in the indirect dimension. It has been demonstrated that adiabatic-passage CP is effective for strongly oriented membrane systems, even at the magic angle [25], but for systems that are particularly sensitive to sample heating or where $T_{1\rho}$ is short, a short CP time optimized for the spinning angle is preferable. In order for VAS and SAS methods to be applied more broadly to samples in the intermediate regime between rigid solids and oriented liquids, it is necessary to consider the behavior of CP at different spinning angles. Many interesting systems fall into this category, including highly mobile solids, semisolids, or hydrogels. However, these samples are complex, often having several components and a strong dependence of their phase behavior on temperature. Therefore, characterization with a well-established model system is necessary. In this letter, we describe simulations and measurements of CP in adamantane over the full range of angles between 0° and 90° in a VAS/SAS probe built for this type of experiment.

2. Theory

CP is most conveniently considered in a doubly rotating frame with the *z*–axis along the direction of the spin lock field. In this frame the total spin Hamiltonian $\hat{H}_{IS}$ for two coupled spins *I* and *S* is given by:

$$\widehat{H}_{IS} = \omega_{1I}\widehat{I}_z + \omega_{1S}\widehat{S}_z + \omega_{IS}2\widehat{I}_x\widehat{S}_x \quad (1)$$

where ω_{1I} and ω_{1S} are the RF nutation frequencies and ω_{1S} the heteronuclear dipolar coupling between an abundant *I* spin and a rare *S* spin.

For a sample spinning at a frequency ω_r and at an angle β_{RL} with respect to the static magnetic field B_0, the heteronuclear dipolar coupling becomes time dependent and is given by:

$$\omega_{IS}(t)=b_{IS}\sum_{n=-2}^{2}D_{0n}^{2}(\Omega_{PR})d_{n0}^{2}(\beta_{RL})e^{in\omega_r t} \tag{2}$$

where $b_{IS}=(\hbar\mu_0/4\pi)\gamma_I\gamma_S r_{IS}^{-3}$ is the dipolar constant, $D_{0n}^{2}(\Omega)$ is an element of the second-rank Wigner matrix, $d_{n0}^{2}(\beta)$ is an element of the second-rank reduced Wigner matrix, and Ω_{PR} is a set of Euler angles describing the relative orientation between the internuclear vector and the rotor axis [26].

The Hamiltonian in Equation 1 can be decomposed into two spin subspaces, a zero-quantum subspace and a double-quantum subspace. In the case where $\omega_{1I}+\omega_{1S}\gg\omega_{IS}$ and $\omega_{1I}-\omega_{1S}\ll\omega_{IS}$, the zero-quantum transition dominates the cross polarization process. The Hamiltonian $\hat{H}_{IS}$ in the zero-quantum subspace is given by:

$$\widehat{H}_{ZQ}=(\omega_{1I}-\omega_{1S})\widehat{I}_z^{ZQ}+\omega_{IS}(t)\widehat{I}_x^{ZQ} \tag{3}$$

where

$$\widehat{I}_z^{ZQ}=\widehat{I}_z-\widehat{S}_z \tag{4}$$

and

$$\widehat{I}_x^{ZQ}=\frac{1}{2}(\widehat{I}_+\widehat{S}_-+\widehat{I}_-\widehat{S}_+) \tag{5}$$

Transforming the $\hat{H}_{ZQ}$ into a frame rotating at the frequency $\omega_\Delta=\omega_{1I}-\omega_{1S}$ we obtain:

$$\begin{aligned}\widehat{H}_{ZQ}^{T}&=\exp\left(i\omega_\Delta t\widehat{I}_z^{ZQ}\right)\widehat{H}_{ZQ}\exp\left(-i\omega_\Delta t\widehat{I}_z^{ZQ}\right)\\&=\omega_{IS}(t)\left[\cos(\omega_\Delta t)\widehat{I}_x^{ZQ}-\sin(\omega_\Delta t)\widehat{I}_y^{ZQ}\right]\end{aligned}$$

As a result, we expect to find a non-vanishing heteronuclear dipolar coupling if

$$\exp(in\omega_r t)\exp(\pm i\omega_\Delta t)=1 \tag{6}$$

leading to the usual condition $\pm\omega_\Delta+n\omega_r=0$.

Moreover, taking into account the angle dependence of the rotor a non-vanishing heteronuclear dipolar coupling will be found if $d_{n0}^{2}(\beta_{RL})\neq 0$, with:

$$d^2_{00}(\beta_{RL}) = \frac{1}{2}\left(3\cos^2(\beta_{RL}) - 1\right)$$
$$d^2_{\pm 10}(\beta_{RL}) = \mp\sqrt{\frac{3}{8}}\sin(2\beta_{RL})$$
$$d^2_{\pm 20}(\beta_{RL}) = \pm\sqrt{\frac{3}{8}}\sin^2(\beta_{RL})$$

Interactions among these give rise to the CP match conditions as well as numerous recoupling conditions. A thorough Floquet treatment of the Hamiltonians involved is available [27], but in this case the relevant interactions can be seen by plotting the elements of the reduced Wigner matrices (Figure 1). At the magic angle, $\beta_{RL} = \arctan\sqrt{2} \simeq 54.74^\circ$ and the reduced Wigner matrix elements vanish for $n = 0$ explaining why the Hartmann-Hahn matching occurs only at n =1,2. For the $n = 0$ condition, transfer can occur via either the J-coupling, or the second-order cross terms between a homonuclear and a heteronuclear coupling. The latter effect has recently been exploited by Lange et al to deliver low-power CP at fast MAS rates [28]. In the case of a mobile sample such as adamantane at the low to moderate spinning speeds of interest here, the J-coupling effect dominates the $n = 0$ condition. Looking at some particular angles, when $\beta_{RL} = 0°$, $d^2_{10}(0^\circ)=0$, $d^2_{20}(0^\circ)=0$, such that the Hartmann-Hahn matching is equivalent to the static case when the sample is spinning parallel to the magnetic field B_0. On the other hand, when $\beta_{RL} = 90°$, $d^2_{10}(90^\circ)=0$ and thus the odd-numbered sidebands disappear from the Hartmann-Hahn match curve.

3. Materials and methods

Adamantane was purchased from Sigma-Aldrich. One-dimensional ^{1}H-^{13}C CP NMR spectra were collected on a 11.7 T wide-bore magnet equipped with a Chemagnetics console and a homebuilt 3.2 mm rotor double-resonance pneumatic SAS NMR probe [29]. All experiments were performed at room temperature using SPINAL decoupling [30]. The CP experiments were done over a range of angles from 0° to 90° which were set using a HGT-3030 Hall effect sensor (Lakeshore) [31]. Simulations were performed using the SIMPSON software [32]. The powder averages were calculated using 320 orientations, selected according to the REPULSION algorithm [33].

4. Results and discussion

Adamantane has a long history in solid-state NMR because its molecular symmetry and fast motions result in its having no chemical shift anisotropy and strongly attenuated heteronuclear and homonuclear dipolar couplings [1, 34, 35]. In this experiment, the RF field applied to the ^{13}C nuclei is held constant at 28 kHz and the RF field applied to the protons is arrayed from 15-55 kHz. The ^{13}C signal intensity is plotted as a function of the applied proton field in Figure 2. The off-magic angle arrays were adjusted to align with the MAS data due to minor differences in probe tuning at different angles. As expected, at the magic angle the $n = +2$ and $n = \pm 1$ sidebands give the strongest signals. For the low-power condition explored here, the $n = -2$ sideband is weak because the efficiency of CP declines at RF amplitudes below 20 kHz. At angles smaller than the magic angle, the center band is more pronounced, and begins to dominate at small spinning angles, resembling the static case at 0°. As described by Sardashti and Maciel [12], the situation at 90° is quite different - the $n = \pm 1$ conditions disappear and the match array is dominated by the $n = 0$ and $n = \pm 2$ bands. The CP maxima at the $n = 0$ and $n = 2$ conditions are significantly broader than the $n = \pm 1$ conditions at the magic angle, making this condition easier to locate in a mobile sample. As expected, a similar set of experiments performed on ^{13}C alanine at $\omega_r = 5$ kHz showed greatly reduced modulation of the signal due to the much stronger ^{1}H-^{1}H dipolar

couplings. In principle, CP transfer is most efficient at 0°. However, good signal intensity is also obtained with CP at 90°, and this may be preferable for some experiments, particularly in the context of separated local field spectra where the spectral width in the indirect dimension is limited by the magnitude of the couplings.

CP match curves for adamantane were also simulated at different spinning angles. The dipole-dipole couplings can be derived assuming that the internal couplings of each adamantane molecule are completely averaged by its fast isotropic rotation, leaving sixteen uncoupled protons in the center of each molecule. These centers form a body-centered tetragonal lattice such that each center has twelve nearest neighbor-centers each at a distance of 6.54 Å [36]. Using the Root-Sum-Square dipolar coupling approximation [37], we can derive the effective dipolar couplings: $D_{HH} = -5950$ Hz and $D_{CH} = -1500$ Hz. The simulated CP match curves resulting from these parameters are shown in Figure 3.

In the fast spinning regime, the ZQ and DQ Hartmann-Hahn conditions are better separated, and either can be used with low-power irradiation to provide frequency-selective CP [38, 39]. Recently, low-power CP with ultra fast MAS has been a topic of intense interest. This is useful in rigid solids where low-power experiments are desired, such as protein nano- or microcrystals. However, we are interested in low-power CP under slow to moderate MAS, as these are the conditions most amenable to semisolid materials and highly mobile solids. In addition to liquid crystals and membranes, this could include surfactants at low water concentration [40] as well as proteins containing both mobile and rigid regions [41]. At the low spinning speeds used here, low-power CP results in inefficient transfer, as observed in the experimental data shown in Figure 2. At values of the RF field strength at or below about 20 kHz, the signal intensity is dramatically reduced or eliminated. The probe used in these experiments is a homebuilt double-resonance VAS/SAS probe in which the B_1 field delivered is independent of the angle [29]. Although this probe can deliver higher RF amplitudes on both channels, the combination of low field and slow spinning is used here with the future intention of investigating membrane systems, hydrogels, and semisolids. In this type of sample, fast spinning is not required for effective decoupling. In fact, in many cases it is detrimental because the ordered components can be centrifuged to the center of the rotor, leading to complex inhomogeneities. These samples are also lossy, such that high RF power or the long pulses required for adiabatic CP may cause significant sample heating.

In order to optimize CP-VAS experiments, it is necessary to consider the time-dependence of the CP buildup as well as the intensity of the signal obtained. In the case of a single proton *I* dipolar coupled to one ^{13}C *S*, the theoretical time-dependence of the transferred S-spin polarization is given by [4]:

$$s(\tau_{CP}) \tilde{=} \sin^2\left[\frac{\omega_{IS} \times \tau_{CP}}{2}\right] \tag{7}$$

Thus, for a single crystal orientation the CP buildup curve follows:

$$s(\tau_{CP}) = \sin^2\left[\frac{\tau_{CP}}{2} b_{IS} d^2_{n0}(\beta_{PR}) d^2_{0n}(\beta_{RL})\right] \tag{8}$$

After powder averaging the buildup curve becomes

$$s(\tau_{CP})=\frac{1}{2}\int_0^{\pi}\sin\left[\frac{\tau_{CP}}{2}b_{IS}\,d_{n0}^2(\beta_{PR})d_{0n}^2(\beta_{RL})\right]^2\sin(\beta_{PR})d\beta_{PR} \tag{9}$$

Eq. 9 provides a theoretical equation describing the CP buildup curves as a function of the spinning angle β_{RL} and the contact time τ_{CP} It has been shown that exact solutions to Eq. 9 can be analytically derived [42, 43]. For example, in the case where $n = 0$, Eq. 9 becomes:

$$s_n=0(\tau_{CP})=\frac{1}{2}-\frac{1}{2x_0}(Fc(x_0)\cos\varphi_0+Fs(x_0)\sin\varphi_0) \tag{10}$$

where

$$x_0=\sqrt{\frac{3\tau_{CP}b_{IS}\,d_{00}^2(\beta_{RL})}{\pi}} \tag{11}$$

$$\varphi_0=\frac{\tau_{CP}}{2}\left(b_{IS}\,d_{00}^2(\beta_{RL})\right) \tag{12}$$

and $Fc(x)$, $Fs(x)$ are the cosine and sine Fresnel integrals

$$Fc(x)=\int_0^x\cos\left(\frac{\pi y^2}{2}\right)dy \tag{13}$$

$$Fs(x)=\int_0^x\sin\left(\frac{\pi y^2}{2}\right)dy \tag{14}$$

Similarly, in the case where $n = \pm 2$, Eq. 9 becomes:

$$s_{n=\pm2}(\tau_{CP})=\frac{1}{2}-\frac{1}{2x_2}(Fc(x_2)\cos\varphi_2+Fs(x_2)\sin\varphi_2) \tag{15}$$

where

$$x_2=\left(\frac{3}{2}\right)^{1/4}\sqrt{\frac{\tau_{CP}b_{IS}\,d_{20}^2(\beta_{RL})}{\pi}} \tag{16}$$

$$\varphi_2 = \frac{\tau_{CP}}{2}\sqrt{\frac{3}{2}}\left(b_{IS}\, d^2_{20}(\beta_{RL})\right) \tag{17}$$

In the case where $n = \pm 1$, Eq. 9 cannot be solved analytically, but must be evaluated numerically.

Fig. 4 compares the theoretical curves obtained form Eq. 9, for $n = 0, \pm 1, \pm 2$, with a series of numerical simulations in which the spinning angle β_{RL} is increased form 40 to 66 degrees. The agreement is excellent in this idealized case.

For a real sample, the situation is more complicated due to the presence of additional spins and the effects of relaxation. Experimental CP buildup curves for the CH_2 resonance of adamantane for the $n = 0$, $n = 1$, and $n = 2$ conditions were collected at different angles (Figure 5). These experimental curves show fewer oscillations than the idealized case of a single C-H pair, as the simulations for this ideal model neglected relaxation effects and ^{1}H-^{1}H dipolar couplings. Furthermore, in the magic angle case, the simulations predict zero intensity for $n = 0$ at the magic angle, which is not the case due to J-couplings and second-order effects neglected in the simulation. Nevertheless, the simulations are useful for making qualitative comparisons. As observed by Wu and Zilm [4], at the magic angle the buildup of magnetization on ^{13}C occurs fastest at the $n = 1$ sideband condition, slightly slower at $n = 2$ and significantly slower at n=0. In agreement with the simulation, on either side of the magic angle at 36° and 66° the magnetization is most intense and has the fastest buildup at the $n = 1$ condition. Comparing the behavior of the $n = 0$ and $n = 2$ conditions away from the magic angle shows faster CP buildup at the $n = 0$ condition for 36° and at the $n = 2$ condition for 67°. At 36°, the difference between n=2 and n=0 is reduced, which can be explained by the matrix elements plotted in Figure 1 d^2_{00} and d^2_{20}, which both approach zero at this angle. At 90°, the fastest buildup is obtained at the $n = 2$ condition. Overall, the slope of the curve for d^2_{20} is less pronounced, making the match at this condition easier to achieve experimentally for a mobile sample.

5. Conclusion

We have measured and simulated the cross-polarization intensity and buildup dynamics over a range of angles from 0° to 90°. For mobile samples, such as adamantane, the CP match condition has a significant dependence on the spinning axis. This is relevant not only to VAS experiments, where CP is performed at every angle, but also to SAS experiments on mobile samples. Our findings show that for off-magic angle conditions, it may be advantageous to use the $n = 0$ or $n = \pm 2$ match conditions, as they are often easier to achieve and result in more a rapid build-up of S-spin polarization. As oriented membrane systems and many other important samples that fall in the regime between rigid solids and isotropic liquids are quite lossy and are therefore prone to overheating when subjected to high RF power or pulses of extended length, minimizing CP contact time is essential. Characterization of CP performance over a broad range of angles is a necessary first step for the development of novel SAS and VAS experiments. The ability to obtain equally good CP signal off the magic angle with proper calibration opens the door to a number of new multidimensional SAS or VAS experiments, since every angle switch entails storing the magnetization along z and losing signal. The ability to perform at CP any angle eliminates the need to switch angles before performing CP and again before detection, allowing more freedom to design multidimensional experiments correlating two anisotropic dimensions or observing the evolution of anisotropic terms in a ^{13}C dimension.

Acknowledgments

This work was supported by NSF CAREER grant CHE-0847375 and NIH R01 GM-78528.

References

1. Pines A, Waugh JS, Gibby MG. Proton-enhanced nuclear induction spectroscopy - method for high-resolution NMR of dilute spins in solids. Journal of Chemical Physics. 1972; 56(4):1776.
2. Schaefer J, Stejskal EO. C-13 nuclear magnetic resonance of polymers spinning at magic angle. Journal of the American Chemical Society. 1976; 98(4):1031–1032.
3. Wind RA, Ded SF, Lock H, Maciel GE. 13C CP MAS and high-speed magic-angle spinning. Journal of Magnetic Resonance. 1988; 79(1):136–139.
4. Wu XL, Zilm KW. Cross polarization with high-speed magic-angle spinning. Journal of Magnetic Resonance, Series A. 1993; 104(2):154–165.
5. Frydman L, Chingas G, Lee Y, Grandinetti P, Eastman M, Barrall GA, Pines A. Variable-angle correlation spectroscopy in solid-state nuclear magnetic resonance. Journal of Chemical Physics. 1992; 97(7):4800–4808.
6. Frydman L, Chingas GC, Lee YK, Grandinetti PJ, Eastman MA, Barrall GA, Pines A. Correlation of isotropic and anisotropic chemical shifts in solids by two-dimensional variable-angle-spinning NMR, Israel. Journal of Chemistry. 1992; 32(2-3):161–164.
7. Bax A, Szeverenyi N, Maciel G. Chemical shift anisotropy in powdered solids studied by 2D FT NMR with flipping of the spinning axis. Journal of Magnetic Resonance. 1983; 55:494–497.
8. Terao T, Fujii T, Onoderra T, Saika A. Switching-angle sample spinning NMR spectroscopy for obtaining powder-pattern-resolved 2D spectra: measurements of 13C chemical shift anisotropies in powdered 3,4-dimethoxybenzaldehyde. Chemical Physics Letters. 1984; 107(2):145–148.
9. Iwamiya J, Davis MF, Maciel G. A 1D FT experiment for obtaining chemical-shift tensors in complex solids, using selective excitation and flipping of the spinner axis. Journal of Magnetic Resonance. 1990; 88:199–204.
10. Terao T, Miura H, Saika A. Dipolar SASS NMR spectroscopy: Separation of heteronuclear dipolar powder patterns in rotating solids. Journal of Chemical Physics. 1986; 85(7):3816–3826.
11. Baltisberger JH, Gann SL, Grandinetti PJ, Pines A. Cross polarization dynamic-angle spinning nuclear-magnetic resonance of quadrupole nuclei. Molecular Physics. 1994; 81(5):1109–1124.
12. Sardashti M, Maciel GE. Effects of sample spinning on cross polarization. Journal of Magnetic Resonance. 1987; 72:467–474.
13. Park SH, Das BB, De Angelis AA, Scrima M, Opella SJ. Mechanically, magnetically, and “rotationally” aligned membrane proteins in phospholipid bilayers give equivalent angular constraints for NMR structure determination. Journal of Physical Chemistry B. 2010; 114:13995–14003.
14. Courtieu J, Alderman DW, Grant DM, Bayles JP. Director dynamics and NMR applications of nematic liquid crystals spinning at various angles from the magnetic field. Journal of Chemical Physics. 1982; 77:723–730.
15. Vaananen T, Jokisaari J, Selantaus M. Variable-angle spinning H-1-NMR spectra of molecules in liquid-crystalline phases with positive and negative diamagnetic anisotropy. Chemical Physics Letters. 1986; 129(4):399–402.
16. Courtieu J, Bayle JP, Fung BM. Variable angle sample spinning NMR in liquid crystals. Progress in Nuclear Magnetic Resonance Spectroscopy. 1994; 26(Part 2):141–169.
17. Beguin L, Courtieu J, Ziani L, Merlet D. Simplification of the 1H NMR spectra of enantiomers dissolved in chiral liquid crystals, combining variable angle sample spinning and selective refocusing experiments. Magnetic Resonance in Chemistry. 2006; 44(12):1096–1101. [PubMed: 16991108]
18. Kummerlöwe G, Grage SL, Thiele CM, Kuprov I, Ulrich AS, Luy B. Variable angle NMR spectroscopy and its application to the measurement of residual chemical shift anisotropy. Journal of Magnetic Resonance. 2011; 209:19–30. [PubMed: 21256060]

19. Zandomeneghi G, Tomaselli M, van Beek JD, Meier BH. Manipulation of the director in bicellar mesophases by sample spinning: A new tool for NMR spectroscopy. Journal of the American Chemical Society. 2001; 123(5):910–913. [PubMed: 11456624]
20. Zandomeneghi G, Tomaselli M, Williamson PTF, Meier BH. NMR of bicelles: orientation and mosaic spread of the liquid-crystal director under sample rotation. Journal of Biomolecular NMR. 2003; 25(2):113–123. [PubMed: 12652120]
21. Kishore AI, Prestegard JH. Molecular orientation and conformation of phosphatidylinositides in membrane mimetics using variable angle sample spinning (VASS) NMR. Biophysical Journal. 2003; 85(6):3848–3857. [PubMed: 14645074]
22. Havlin RH, Park GHJ, Pines A. Two-dimensional NMR correlations of liquid crystals using switched angle spinning. Journal of Magnetic Resonance. 2002; 157(1):163–169. [PubMed: 12202147]
23. Havlin R, Park G, Mazur T, Pines A. Using switched angle spinning to simplify NMR spectra of strongly oriented samples. Journal of the American Chemical Society. 2003; 125(26):7998–8006. [PubMed: 12823022]
24. Zandomeneghi G, Williamson PTF, Hunkeler A, Meier BH. Switched-angle spinning applied to bicelles containing phospholipid-associated peptides. Journal of Biomolecular NMR. 2003; 25(2): 125–132. [PubMed: 12652121]
25. Zandomeneghi G, Meier BH. Adiabatic-passage cross polarization in N-15 NMR spectroscopy of peptides weakly associated to phospholipids: Determination of large RDC. Journal of Biomolecular NMR. 2004; 30(3):303–309. times Cited: 2. [PubMed: 15754056]
26. Eden M. Computer simulations in solid-state NMR. I. spin dynamics theory. Concepts in Magnetic Resonance, Part A. 2003; 17:117–154.
27. Scholz I, Meier BH, Ernst M. Operator-based triple mode Floquet theory in solid-state NMR. Journal of Chemical Physics. 2007; 127:204504. [PubMed: 18052439]
28. Lange A, Scholz I, Manolikas T, Ernst M, Meier BH. Low-power cross polarization in fast magic-angle spinning NMR experiments. Chemical Physics Letters. 2009; 468(1-3):100–105.
29. Litvak IM, Espinosa CA, Shapiro RA, Oldham AN, Duong VV, Martin RW. Pneumatic switched angle spinning NMR probe with capacitively coupled double saddle coil. Journal of Magnetic Resonance. 2010; 206:183–189. [PubMed: 20673643]
30. Fung BM, Khitrin AK, Ermolaev K. An improved broadband decoupling sequence for liquid crystals and solids. Journal of Magnetic Resonance. 2000; 142(1):97–101. [PubMed: 10617439]
31. Mamone S, Dorsch A, Johannessen OG, Naik MV, Madhu PK, Levitt MH. A Hall effect angle detector for solid-state NMR. Journal of Magnetic Resonance. 2008; 190(1):135–141. [PubMed: 17910927]
32. Bak M, Rasmussen JT, Nielsen NC. SIMPSON: A general simulation program for solid-state NMR spectroscopy. Journal of Magnetic Resonance. 2000; 147(2):296–330. [PubMed: 11097821]
33. Bak M, Nielsen NC. REPULSION, a novel approach to efficient powder averaging in solid-state NMR. Journal of Magnetic Resonance. 1997; 125(1):132–139. [PubMed: 9245368]
34. Garroway AN. Homogeneous and inhomogeneous nuclear spin echoes in organic solids: Adamantane. Journal of Magnetic Resonance. 1977; 28:365–371.
35. Bronniman CE, Szeverenyi NM, Maciel GE. 13C spin diffusion of adamantane. Journal of Chemical Physics. 1983; 79:3694–3700.
36. Nowacki W. Die krystallstruktur von adamantan (symm. tri-cyclodecan). Helvetica Chimica Acta. 1945; 104:293–304.
37. Zorin VE, Brown SP, Hodgkinson P. Quantification of homonuclear dipolar coupling networks from magic-angle spinning H-1 NMR. Molecular Physics. 2006; 104(2):293–304.
38. Meier BH. Cross polarization under fast magic angle spinning - thermodynamical considerations. Chemical Physics Letters. 1992; 188(3-4):201–207.
39. Laage S, Marchetti A, Sein J, Pieratelli R, Sass H, Grzesiek S, Lesage A, Pintacuda G, Emsley L. Band-selective 1H-13C cross-polarization in fast magic angle spinning solid-state NMR spectroscopy. Journal of the American Chemical Society. 2008; 130:17216–17217. [PubMed: 19053413]

40. Nowacka A, Mohr P, Norrman J, Martin RW, Topgaard D. Polarization transfer solid-state NMR for studying surfactant phase behavior. Langmuir. 2010; 26:16848–16856. [PubMed: 20925371]

41. Helmus JJ, Surewicz K, Nadaud PS, Surewicz WK, Jaroniec CP. Molecular conformation and dynamics of the Y145Stop variant of human prion protein in amyloid fibrils. Proceedings of the National Academy of Sciences of the United States of America. 2008; 105:6284–6289. [PubMed: 18436646]

42. Pileio G, Guo Y, Pham T, Griffin J, Levitt M, Brown S. Residual dipolar couplings by off-magic-angle spinning in solid-state nuclear magnetic resonance spectroscopy. Journal of the American Chemical Society. 2007; 129(36):10972–10973. [PubMed: 17705478]

43. Thureau P, Sauerwein AC, Concistre M, Levitt MH. Selective internuclear coupling estimation in the solid-state NMR of multiple-spin systems. Phys Chem Chem Phys. 2011; 13:93–96. [PubMed: 20967326]

Highlights

- In mobile solids, dipolar couplings are modulated as a function of spinning angle.
- The modulation affects the intensity and rate of cross polarization (CP).
- These effects have been simulated and measured from 0 degrees to 90 degrees.
- Good CP intensity can sometimes be more easily obtained away from the magic angle.
- CP must be optimized at different angles to develop new SAS and VAS experiments.

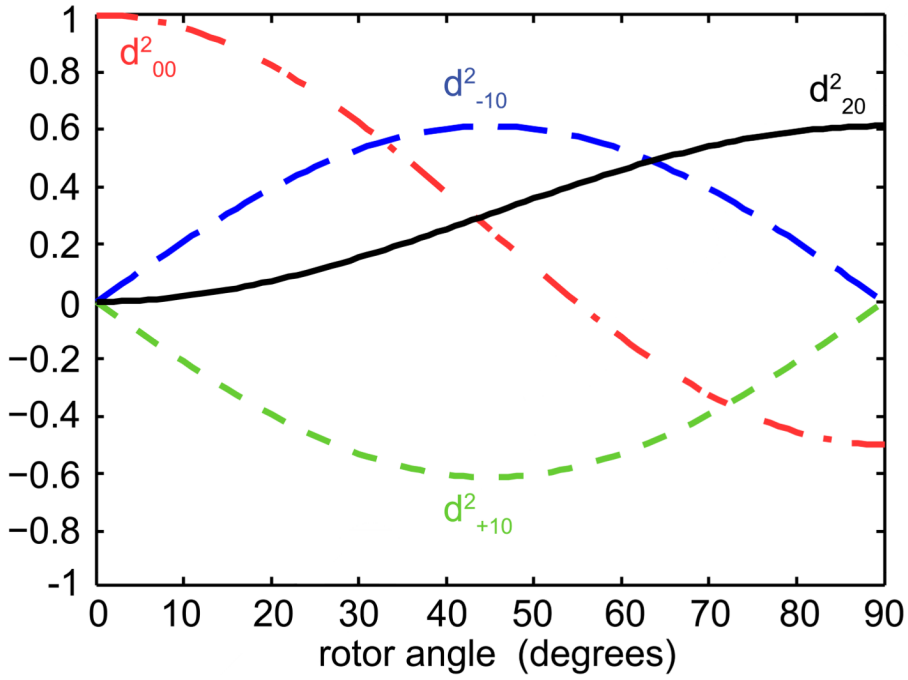

Figure 1.

The elements of the reduced Wigner matrices are plotted as a function of rotor angle, with 1 being the maximum theoretical transfer efficiency, observed at 0° (the static case). At the magic angle, the d^2_{-10} and d^2_{+10} terms dominate, although the contribution from the d^2_{20} term is also significant (d^2_{-20} is not plotted here because the low-power CP conditions used in the experiment did not permit observation of polarization transfer by this mechanism in the measured data). At 90°, the d^2_{-10} and d^2_{+10} terms vanish, leaving only the d^2_{00} and d^2_{+20} terms. Although the maximum theoretical transfer is not achieved away from 0°, it can easily be seen that the intensity obtained from d^2_{20} at 90° is comparable to that of the d^2_{-10} and d^2_{+10} terms at the magic angle.

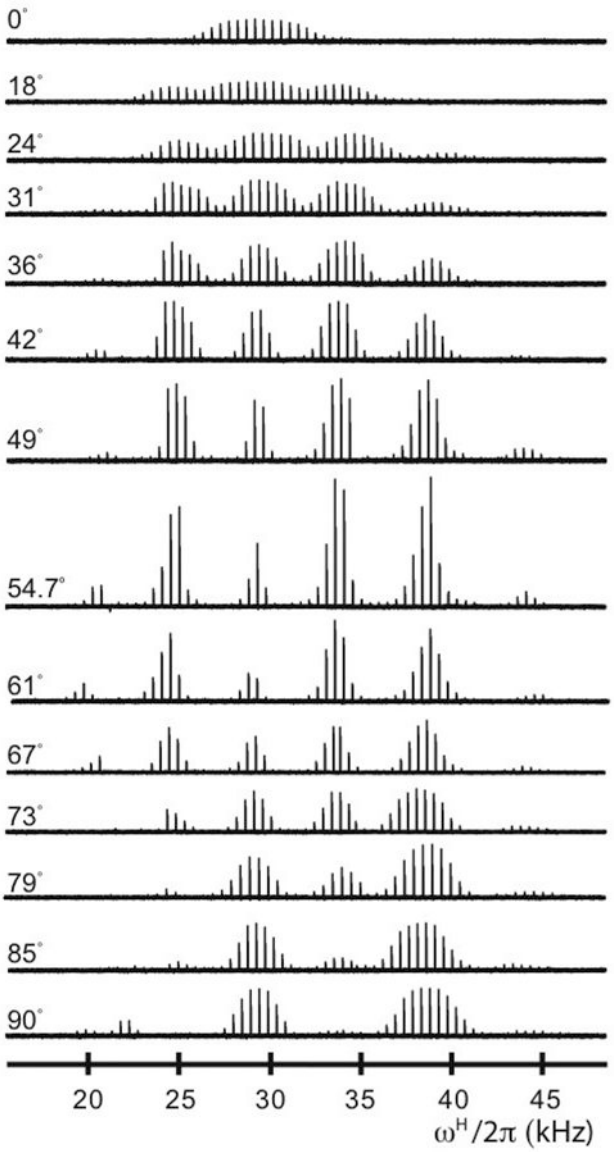

Figure 2.

Experimental ^{1}H-^{13}C cross-polarization arrays of adamantane at different spinning angles. The ^{13}C RF field strength was held constant at 28 kHz and the ^{1}H nutation frequency was arrayed from 15-55 kHz. The rotor frequency was 5 kHz at all angles. The ^{1}H 90° pulse length was 5.5 μs, corresponding to a ^{1}H power of 45.45 kHz).

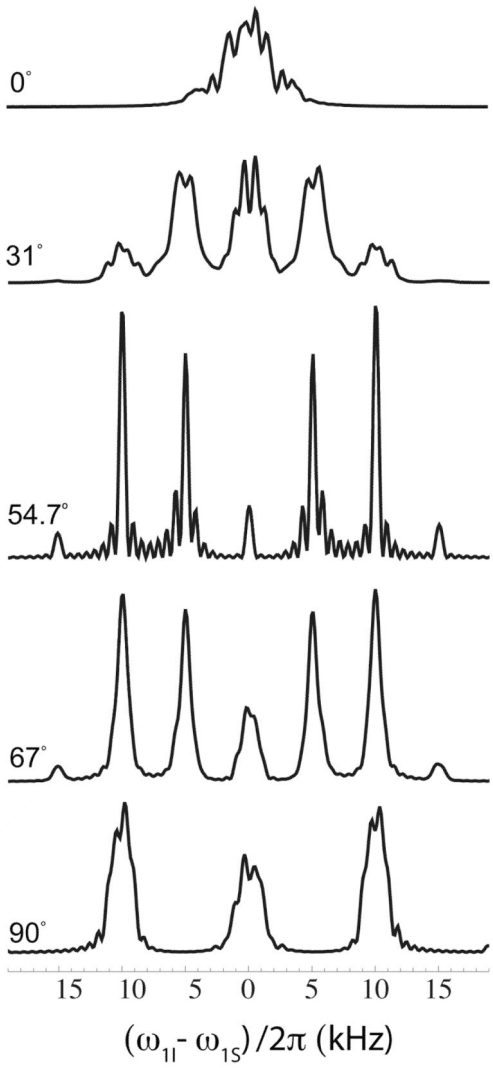

Figure 3.
Simulated ^{1}H-^{13}C cross-polarization arrays for the CH peak of adamantane as a function of spinning angle, under the same conditions as the experiment. Overall, the results are in agreement with the experimental data, except for the the n=-2 match condition, which is not observed in the measured spectra.

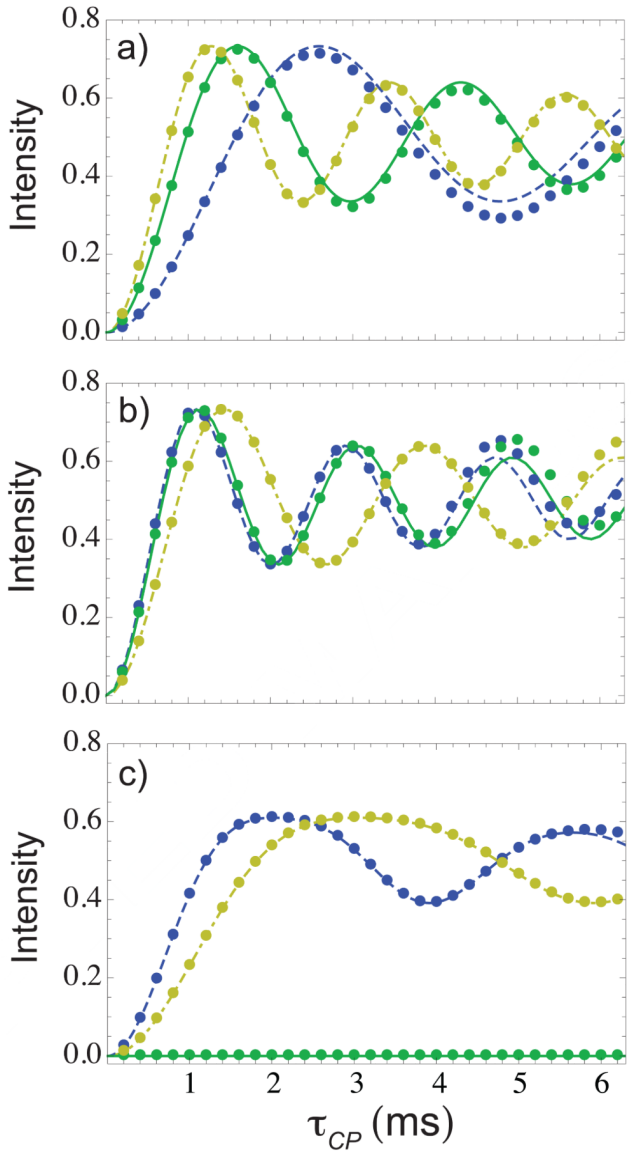

Figure 4.

Dependence of the CP signal intensity on the contact time τ_{CP} at different spinning angles β_{RL}, for two coupled spins I and S a) Numerical simulations with a dipolar coupling constant $b_{IS} = -1500$ Hz (-3000 π radians/second) for the CP conditions $\omega_\Delta = \pm 2\omega_r$ and spinning angles $\beta_{RL} = 40°$ (blue circles), β_{RL} = Magic Angle (green circles) and $\beta_{RL} = 66°$ (yellow circles). b) same as a) but for the CP conditions $\omega_\Delta = \pm\omega_r$. c) same as a) but for the CP conditions $\omega_\Delta = 0$. The theoretical curves obtained from Eq. 9, with a dipolar coupling constant $b_{IS} = -1500$ Hz, are shown by a solid green curve when β_{RL} = Magic Angle, by a dashed blue curve when $\beta_{RL} = 40°$ and by a dot-dashed yellow curve when $\beta_{RL} = 66°$.

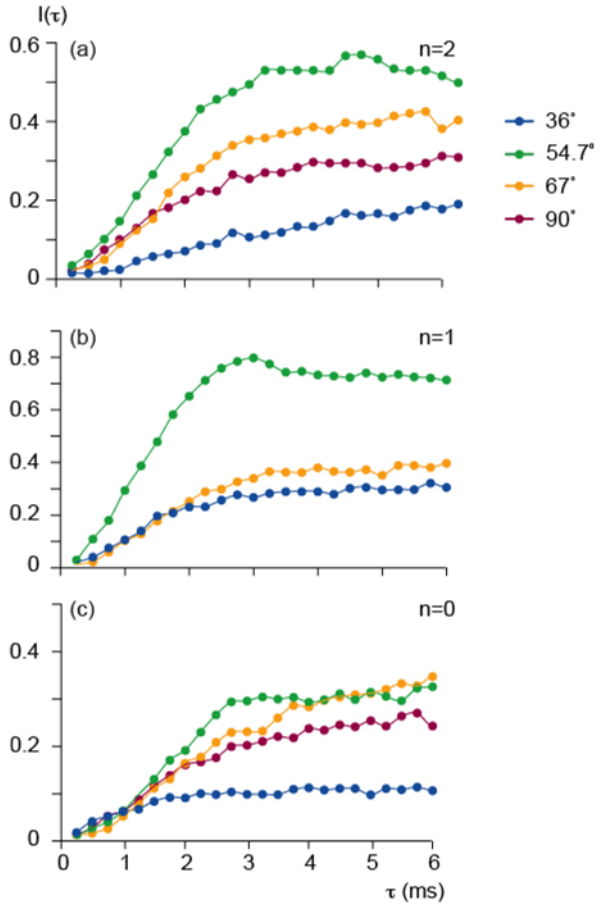

Figure 5.
Contact time arrays for relatively short CP times at different spinning angles. The peak intensity of the CH_2 carbon resonance of adamantane is plotted as a function of contact time for **(a)** $n = 2$ **(b)** $n = 1$ and **(c)** $n = 0$.